Pseudoreflection from interface between two oscillatory media: Extended driver

M. Gutman,[1] I. Aviram,[2] and A. Rabinovitch[1]

[1]*Physics Department, Ben-Gurion University of the Negev, Beer-Sheva 84105, Israel*
[2]*35 Shederot Yeelim, Beer-Sheva 84730, Israel*

The dynamics of a reaction-diffusion medium composed of two uniform self-oscillating regions is considered. We analyze the phenomenon of pseudoreflection of waves at the region's interface. The reflected waves show an unusual change of wavelength, amplitude, and period. In contrast to our previous results, here this behavior can be perceived as an action of a spatially extended higher-frequency "driver." Observed also are the interesting phenomena of the appearance of narrow transient zones near the interface and of diffusion-induced bifurcations. Furthermore, the pseudoreflection is shown to be a possible mechanism of spiral and "target" waves generation. The relevance of the obtained results to the dynamics of the cardiac sinus node is discussed.

I. INTRODUCTION

Limit cycle (LC) media which are similar to a continuum of coupled nonlinear oscillators are widespread in physical, chemical, and biological systems [1–8]. Most of them (e.g., the sinus node in the heart, or the small intestine) are strongly nonuniform LC media of nonidentical oscillators with different natural frequencies. As a suitable model for such oscillators and nonuniformities we use a LC medium composed of two uniform, spatially adjacent regions with different frequencies. Despite its simplicity this model allows us to simulate many interesting phenomena such as the appearance of propagating waves and their *pseudoreflection* from the interface between regions. Along with the usual reversal of propagation direction, these pseudoreflected waves (PRW) exhibit the *unusual* phenomena of a decrease in the wavelength, the amplitude, and the period of oscillations. These features, especially the decrease in period, indicate the existence of higher-frequency sources of the PRW. The PRW phenomenon has previously been observed [9,10] for a *uniform* LC medium of limited size, with various boundary conditions. In both these works, the source (driver) is autonomous (self-generated) and appears inside the LC region, close to the boundary, as a result of the interaction between diffusion and the boundary condition. The PRW are generated via frequency locking of coupled oscillators.

A more complicated case of PRW generation is examined in this work. In contrast to our pervious studies, the *entire* high frequency region must now be considered as an "external" spatially extended driver of PRW driven into the low frequency region. The properties of the high frequency region can now be modified "externally" by varying its size and natural frequency, thus inducing profound changes in the driven PRW, such as (a) different entrainment frequency ratios between the PRW and the driver, and (b) the appearance of a complex transient zone around the region interface. In addition, the high frequency region displays intricate dynamics.

In order to gain a better understanding of the complex dynamics of the model, simplified versions thereof, including different external local drivers, were also investigated. Thus we have analyzed a model of two unidirected coupled oscillators whose properties correspond to the two adjacent, uniform LC regions, and an even simpler model where external perturbations are periodically applied to a single oscillator corresponding to the low-frequency region. The simulation results allow us to explain the most important features of the spatially extended driver.

In addition, the pseudoreflection in two-dimensional space is also briefly considered. The absence of the usual reflection law for the PRW and the generation of spiral waves are observed. Possible applications are also discussed.

II. PRW IN A DUAL ONE-DIMENSIONAL SELF-OSCILLATING MEDIUM

We investigate the propagation of waves in a one-dimensional (1D) reaction-diffusion LC medium which is divided into two uniform space regions at a selected interface point x_0. For this purpose we solve the FitzHugh-Nagumo (FHN) equations [11]:

$$\frac{\partial \nu}{\partial t} = D\frac{\partial^2 \nu}{\partial x^2} + \nu(\nu-a)(1-\nu) - w,$$

$$\frac{\partial w}{\partial t} = \varepsilon(\nu - dw) \tag{1}$$

where $\varepsilon = \varepsilon_2$ if $x \leq x_0$, and $\varepsilon = \varepsilon_1$ if $x > x_0$. We set $\varepsilon_2 > \varepsilon_1$. Here $\nu(x,t)$ stands for an *activator*, embodying, e.g., the *action potential* in the sinus node of the heart while $w(x,t)$ is an *inhibitor*, or a *refractoriness* function. D is the diffusion coefficient, a is the excitability parameter, and ε is a (usually small) parameter measuring the ratio between the time constants of the activator and the inhibitor; d is a parameter. The time t is measured in units of the activator time constant. Neumann boundary conditions are imposed at both ends of the integration domain. The natural frequency of a FHN oscillatory medium is directly related to the magnitude of its ε: in the range of small values of ε, the larger is ε, the higher will be the frequency. The two regions of space are interchangeably specified by their ε value, or by their frequency magnitude.
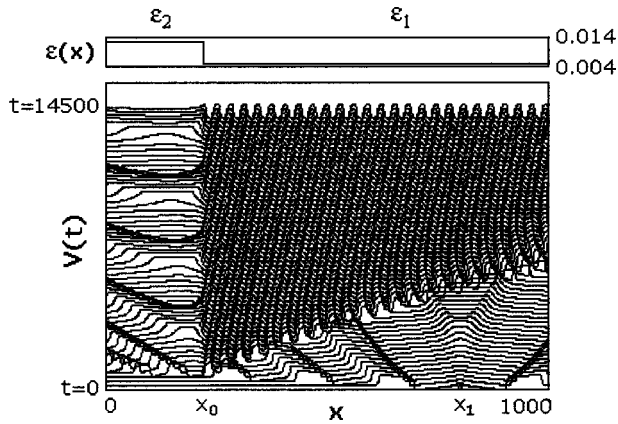
FIG. 1. A stroboscopic picture of propagating and pseudoreflected waves (PRW) in a LC medium with piecewice constant nonuniformity ($\Delta\varepsilon = \varepsilon_2 - \varepsilon_1 = 0.0076$; the time difference between strobes is 228 time units). Firstly, only regular waves are visible propagating in the low-frequency region away from $x = x_1 = 800$, where a localized initial pulse was launched. Then the left-propagating waves reach the high frequency region which starts to generate opposite moving PRW. These are annihilated by collisions with the regular waves. However, the frequency of the PRW being higher, the point of annihilation gradually shifts towards the right edge of the low-frequency region, and after a long time, only PRW are observed. Meanwhile in the left region, the local "source" of the refractive waves slowly moves away from the interface, and a monotonic increase of their wavelength is visible.
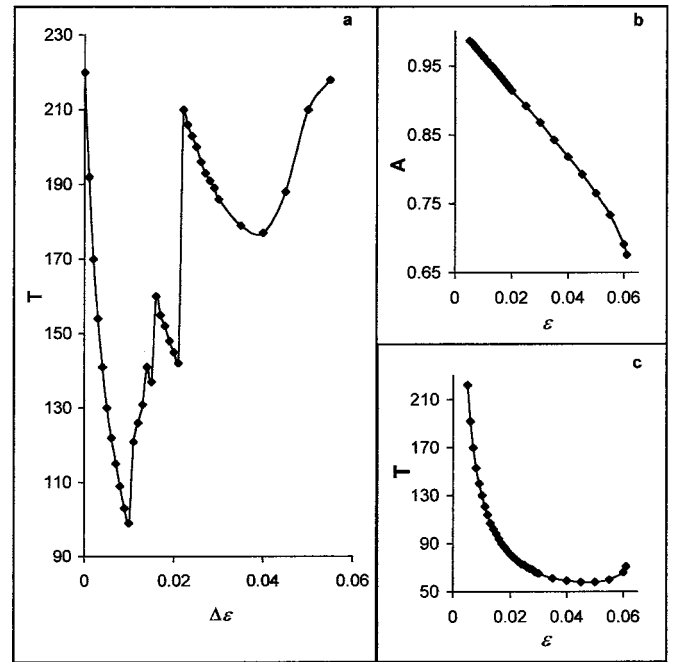

FIG. 2. (a) The period T of the pseudoreflected waves as a function of $\Delta\varepsilon$ (the difference between ε values in the two uniform regions). ε_1 is kept constant at 0.005; (b) the amplitude A and (c) the period T of a *single* oscillator as functions of the parameter ε, correspondingly ($d = 3, D = 1$).

Let us recall (see, e.g., [12]) that a may be either positive or negative; if $\varepsilon \ll 1$ (the relaxation oscillator [13]), and a is negative below a certain threshold value, the system will be in a limit-cycle regime, whereby pulses are autonomously, and periodically generated producing two trains of pulses symmetrically propagating outwards from the location of an initiating pulse with ever increasing wavelength [14,15]. We use the value $a = -0.16$ throughout this work which puts the system in a LC regime. The parameters a, d, D are the same for both regions of space. Note that all parameters and variables are dimensionless.

The numerical integration of the system (1) was carried out using the unconditionally stable Crank-Nicolson method. The values of time and space intervals, used for all numerical experiments, were $\Delta t = 1$ and $\Delta x = 1$. Control runs carried out with smaller grid values invariably showed the same results.

An initiating pulse $v_0(x)$, usually a narrow space Gaussian centered at some $x = x_1(>x_0)$ in the low frequency region, is launched at $t = 0$. As long as the wave train has not reached the regions' interface, a wavelength spreading is observed due to local diffusion currents which tend to minimize the phase differences between adjacent oscillating points. After reaching the interface, point x_0 in the dual medium, it is seen that the left-going waves, which propagated from the ε_1 region, gradually disappear and are replaced by higher frequency right-going waves "reflected" from the interface; see Fig. 1. The actual wave generation process at the interface is as follows: the immediate left vicinity of the interface x_0 begins oscillating at the higher frequency, thus reaching the

maximum amplitude in advance of its nearest neighbors. A diffusion current is therefore created in both directions. This immediate vicinity starts operating as a high frequency external driver for the right hand side region. In due course, through the process of frequency locking, only uniform pseudoreflected waves with a fixed wavelength propagate to the right throughout the whole ε_1 region. Simultaneously in the ε_2 region, waves propagate to the left with spreading wavelength. As a result, after a long transient period, all ε_2 region points collectively operate as an extended unidirectional driver (see below), oscillating with just about their natural frequency, and a minimal phase lag which decreases monotonically from the interface towards the left outer edge.

The value of ε_1 is kept constant at 0.005 in all simulations of the two region model, and the period of the pseudoreflected waves propagating in the ε_1 region is presented in Fig. 2(a) as a function of $\Delta\varepsilon$, where $\Delta\varepsilon = \varepsilon_2 - \varepsilon_1$. For comparison, the period and amplitude of a separate single oscillator versus ε are shown in Figs. 2(b) and 2(c). The observed complex and nonmonotonic behavior in Fig. 2(a) can be explained as entrainment by the external driver. The driver's action becomes clear from Fig. 3, where the frequency of the PRW divided by the frequency of the oscillations in the ε_2 region is displayed as a function of $\Delta\varepsilon$. The obtained picture resembles a portion of a Devil's staircase where comparatively long intervals of strong resonances 1:1, 1:2, and 1:3 appear, and are separated by a set of weak resonances, partially obeying a Farey tree rule. Note that the absence of higher strong resonances is quite reasonable, since a frequency-locking mechanism allows only the propagation of waves whose period is smaller than the natural
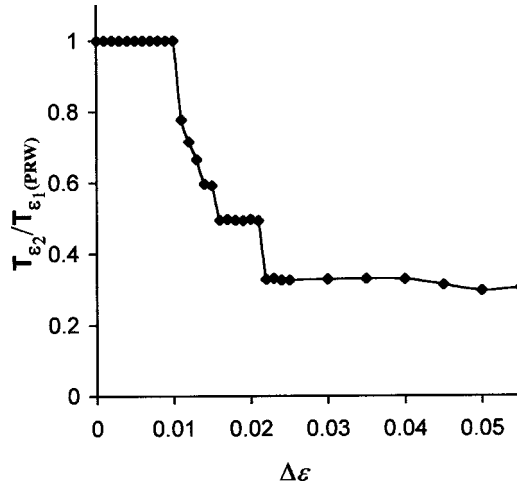
FIG. 3. The ratio $T_{\varepsilon 2}/T_{\varepsilon 1(\mathrm{PRW})}$ between the period of the oscillations in the ε_2 region and the final period of the PRW, as a function of $\Delta\varepsilon$. Entrainments for different rational values of the abscissa are visible showing relatively long horizontal segments corresponding to strong resonances (1:1, 1:2, and 1:3). Also present are several intermediate weak resonances ($d=3$, $D=1$).

period of the ε_1 region (220 dimensionless units in this case). On the other hand, the minimal period of an external driver (region ε_2) is 58 dimensionless units, see Fig. 2(c), implying that the highest integer which, multiplied by 58, yields a value smaller than 220 is 3. Correspondingly, 1:3 is the maximal strong resonance that can be generated here.

It is well known that a similar entrainment driving is generally observed in the dynamics of forced nonlinear single oscillators (see, e.g., [16–18]). To relate such a behavior to our spatially extended case, we "removed" the spatial dependence by considering a system of two unidirected coupled oscillators whose parameters are the same as those of the two uniform regions discussed above. The system of equations is

$$\frac{\partial \nu_1}{\partial t} = K(\nu_2 - \nu_1) + \nu_1(\nu_1 - a)(1 - \nu_1) - w_1,$$

$$\frac{\partial w_1}{\partial t} = \varepsilon_1(\nu_1 - dw_1),$$

$$\frac{\partial \nu_2}{\partial t} = \nu_2(\nu_2 - a)(1 - \nu_2) - w_2,$$

$$\frac{\partial w_2}{\partial t} = \varepsilon_2(\nu_2 - dw_2). \tag{2}$$

Unidirectionality here means that oscillator 2 influences oscillator 1 through the coupling term $K(\nu_2 - \nu_1)$, but not the other way round. The ratio of the final frequencies of the two oscillators versus $\Delta\varepsilon$ is shown in Fig. 4(a). The similarity with Fig. 3 is quite evident.

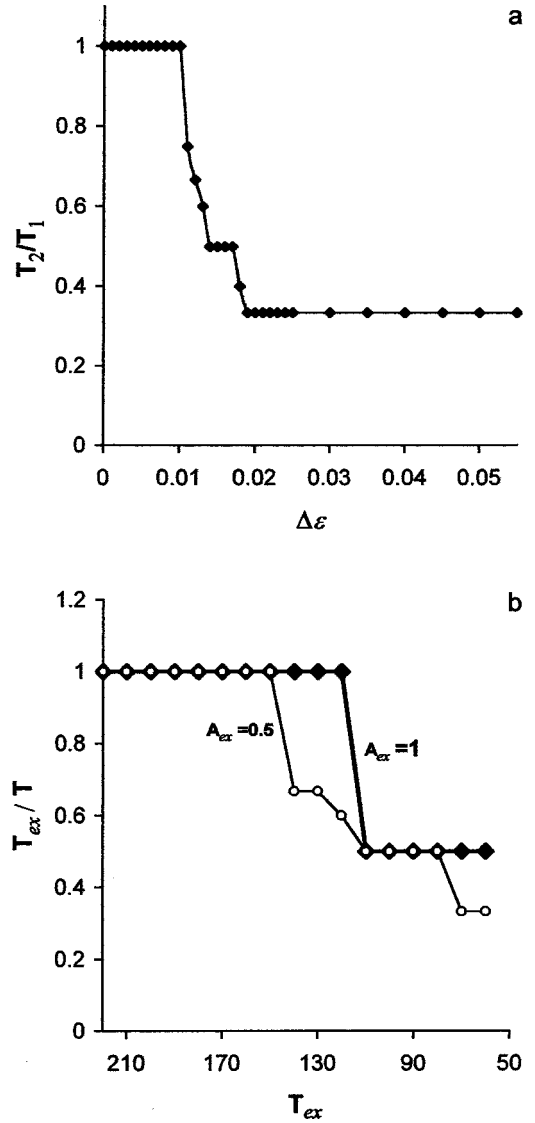An even simpler model was also considered including a single periodically driven oscillator,

FIG. 4. Entrainment (a) in the model of two unidirectionally coupled oscillators, and (b) in the model of a single oscillator with external periodic driving. (a) T_2/T_1 represents the ratio between periods of the driving and driven oscillators, $\Delta\varepsilon = \varepsilon_2 - \varepsilon_1$, and $K = 0.068$; (b) T_{ex}/T represents the ratio between the periods of the external pulses and the driven single oscillator as a function of T_{ex}. The symbols represent the driving amplitude: ■ for $A_{ex} = 1$ and ○ for $A_{ex} = 0.5$ ($d = 3$, $D = 1$).

$$\frac{\partial \nu}{\partial t} = \nu(\nu - a)(1 - \nu) - w + A_{ex} \sum_{m=0}^{\infty} \delta(t - mT_{ex}),$$

$$\frac{\partial w}{\partial t} = \varepsilon(\nu - dw), \tag{3}$$

where A_{ex} is the external driver's amplitude and δ is the Dirac delta function. The period of the oscillator T depends monotonically on the period of the external pulses T_{ex}, while the dependence on A_{ex} is stepwise, Fig. 4(b). These results allow us to qualitatively explain the nonmonotonic dependence of the PRW period versus $\Delta\varepsilon$ presented in Fig.
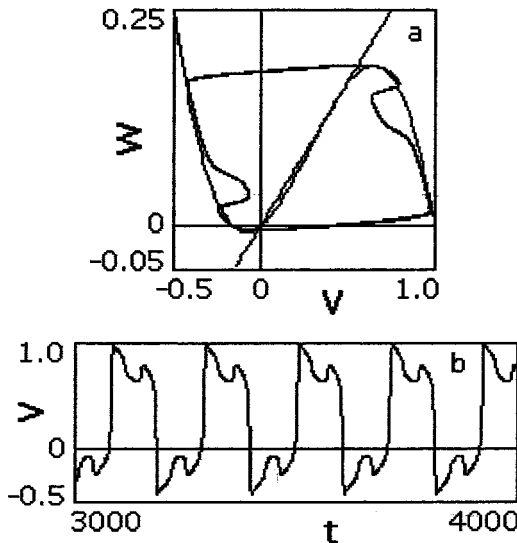
FIG. 5. The phase portrait (a) and the time evolution $\nu(t)$ (b) of the driven oscillator in the model of two unidirectionally coupled oscillators [Eqs. (2)]. The parameters $K=0.068$ and $\Delta\varepsilon=\varepsilon_2-\varepsilon_1$ $=0.0215$ correspond to the 1:3 resonance. Other parameters are the same as in the low-frequency region of the model of Eqs. (1).

2(a). Indeed, an increase of $\Delta\varepsilon$ results in both, a monotonic decrease of the driving amplitude, and a nonmonotonic decrease of its period, cf. Figs. 2(b) and 2(c). Since these two factors have an opposite and nonproportional influence on the PRW period, the nonmonotonic dependence on $\Delta\varepsilon$ becomes reasonable.

III. DIFFUSION INDUCED BIFURCATIONS IN A TRANSIENT ZONE

We note in the model of Eq. (2) that for a comparatively large $\Delta\varepsilon$ ($\Delta\varepsilon \geq 0.01$, beyond the 1:1 resonance) the driven oscillator exhibits complex periodic oscillations, including a few different local maxima, Fig. 5. With the same parameter values, similar oscillations are observed at the point x_0+4, near the border of the low frequency region of the full model, Fig. 6(b). However, the action of diffusion here results in the interesting phenomenon of a gradual "simplification" of these wave forms, i.e., a transition to less intricate wave profiles. Thus, in the low-frequency region there appears a narrow transient zone [about ten grid points from x_0+1, Fig. 6(a), to x_0+10, Fig. 6(c)] where this effect is observed. Beyond this zone, all region points display simple periodic oscillations with equal frequency and constant phase lags.

Different oscillations of neighboring points are obviously possible only when the diffusion coupling is comparatively weak. Our simulations demonstrate that an increase of the diffusion coefficient D causes a proportional decrease of the difference between the complex oscillations at point x_0+1 and its close neighborhood. This is reasonable since an increased coupling between the medium points leads to a more effective "driving" from the point x_0+1 and, as a result, to an increase of the transient zone's size. However, a diffusion-induced bifurcation at the point x_0+1 occurs for $D=5$,
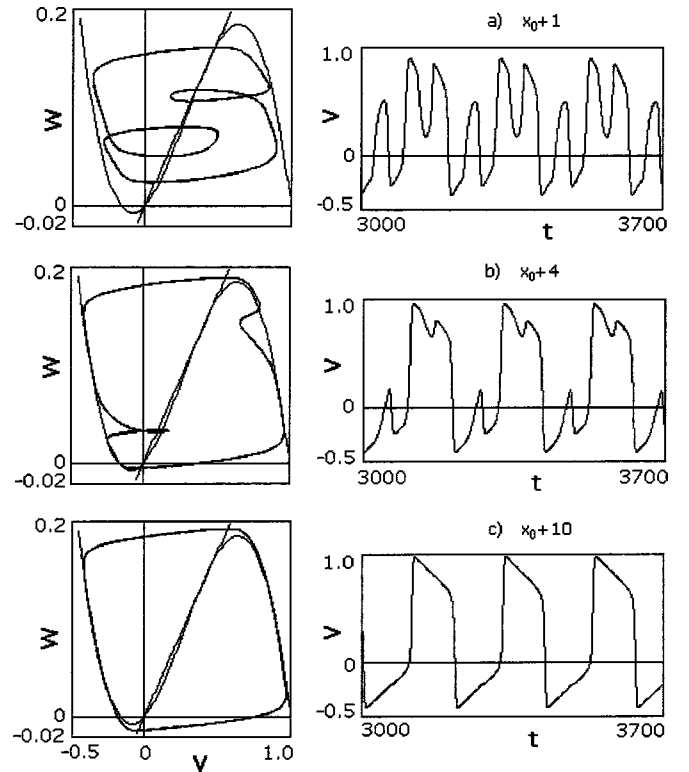

FIG. 6. Phase portraits and time evolutions $\nu(t)$ of the oscillations at three different points in the transient zone of the low-frequency ε_1 region ($\Delta\varepsilon=\varepsilon_2-\varepsilon_1=0.0215$). (a) Complex, period-3 oscillations at the point x_0+1 (the border of the ε_1 region); (b) oscillations of lower complexity at an intermediate point x_0+4; (c) "simplest," period-1 oscillations at the point x_0+10 ($d=3, D=1$).

above which the entrainment changes from (1:3) to (1:2). This entrainment transition simplifies the oscillations profile at the point x_0+1, as well as in the entire transient zone, whose size decreases correspondingly. With a further increase of D, the periodicity of the zone's oscillations is preserved, but its size starts to increase again until a second diffusion-induced bifurcation occurs. Examples of D values corresponding to different oscillations at the point x_0+1 are shown in Fig. 7. Note that oscillations of complex periodicity surprisingly appear between the period 2 and the period 1, Fig. 7(c). Here complex motion in the vicinity of the unstable fixed point $\nu=w=0$ is observed, namely the influence of the fixed point leads to the appearance of three additional phase loops of which one is small, while the other two are large. A further increase of D results in a displacement of the phase trajectories away from the fixed point, and a corresponding oscillation "simplification," Fig. 7(d).

Additional numerical experiments were conducted in which localized external triggering pulses were applied to uniform LC media. No transient zone was observed in these instances, indicating that such transience is a phenomenon peculiar to the spatially extended driver.

IV. DYNAMICS OF THE 1D HIGH FREQUENCY REGION

The collective dynamics of oscillating points belonging to the ε_2 high frequency region is presented in Fig. 8. "Refrac-
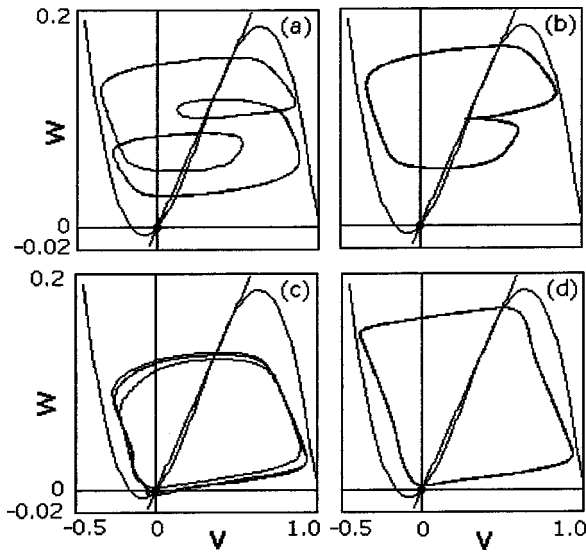
FIG. 7. Diffusion-induced bifurcations at the point $x_0 + 1$ (border of the ε_1 region). (a) Period-3 oscillations for $D = 4$; (b) period-2 oscillations for $D = 5$; (c) period-4 oscillations for $D = 150$. A complex motion is observed around the unstable fixed point (origin of the phase plane) whose influence leads to the appearance of three additional closed loops; (d) period-1 oscillations at $D = 500$. The additional closed loops vanish because the motion takes place further away from the origin. Results are presented for the ε_1, ε_2 regions whose sizes equal 130 and 70 grids points correspondingly ($d = 3$).
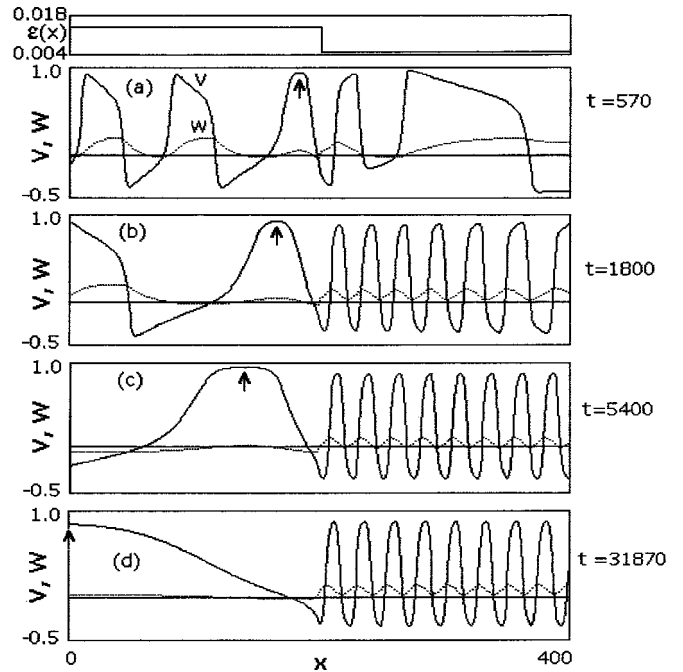

FIG. 8. Dynamics in the high-frequency region: Presented are refractive waves whose wavelength gradually increases with time. Arrows indicate the local "source" of these waves which moves away from the interface. After a long time [frame (d)] only one half of a refractive wave is observed ($d = 3, D = 1$).

tive" waves with a monotonous wavelength spreading are present in this region. A similar phenomenon was also observed previously in uniform LC media [14,15], and explained by "phase locking" of coupled identical oscillators which tend to oscillate in unison i.e., with the same frequency, and zero phase lag. Here, however, an additional transient motion of the local "source" of the refractive waves is observed. This source, defined as the point from which waves propagate in both directions, displays a slow motion across the whole ε_2 region from the interface to the left edge. As a result of the Neumann boundary conditions only one-half of the refractive wave eventually subsists, Fig. 8(d), i.e., the points on the two opposite ends of the region oscillate with a maximal phase lag of 180°. This behavior of the high-frequency region is obtained for a wide range of $\Delta\varepsilon$ values and for different region sizes. The entire region thus acts as a spatially extended driver.

A narrow transient zone of about ten grid points also appears in the ε_2 region, to the left of the interface. The points of this zone have different oscillating amplitudes than the rest of the region. In the case of a comparatively small $\Delta\varepsilon$ (i.e., for the 1:1 resonance) all points of the ε_2 transient zone oscillate with the same frequency but with a gradual increase in the amplitude of oscillations away from the regions' interface. Increasing $\Delta\varepsilon$ brings about more intricate patterns where points belonging to the transient zone display oscillations of different periodicity and complexity. For example, for $\Delta\varepsilon = 0.026$ corresponding to the 1:3 resonance, a gradual transition is observed from complex (period 3) to simple (period 1) types of oscillations.

Note that in order to synchronize the motion of points with different limit cycles, relatively large diffusion currents are required. Therefore a relatively large spatial gradient of ν is observed mainly in the transient zone [see Fig. 8(a)]. This fact might also provide an understanding of the motion of the refractive waves source in Figs. 8(a)–8(d). Indeed, the maximal spatial gradient of ν observed initially in the transient zone, Fig. 8(a), gradually decreases via a diffusion current, Figs. 8(b) and 8(c). This leads to a "smoothing" of the trailing front of the corresponding refractive wave, and thus to the motion of the peak (i.e., the local source) away from the interface.

V. THE EXTENDED DRIVER

It is also found that an increase in size of the higher-frequency region increases its influence on the driven region. Such a dependence of the reflected wave period is monotonic for a comparatively small $\Delta\varepsilon$, as shown in Fig. 9. In the case of a small size of region ε_2, the ensuing frequency is similar to the natural frequency of the ε_1 region. Increasing this size results in a stronger influence, whereby the period is lowered until the corresponding value of the PRW period, shown in Fig. 2, is achieved asymptotically. The PRW dynamics is therefore determined not only by local oscillations at the interface, but by the size of the entire high frequency region
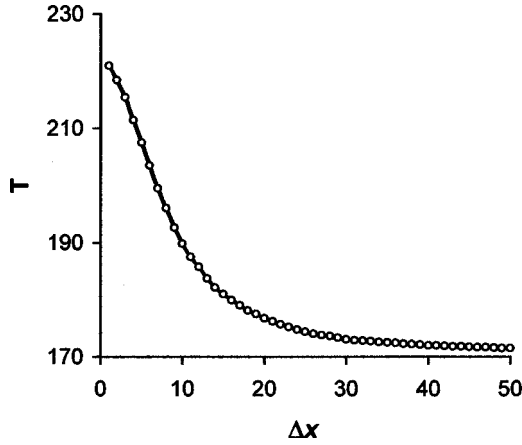
FIG. 9. Final period T of synchronized oscillations in the *entire* medium as a function of the size Δx of the high-frequency region, $\Delta \varepsilon = 0.002$ ($d=3$, $D=1$).

as well. Our hypothesis of a spatially extended driver thus gains ample support.

VI. A TWO-DIMENSIONAL MODEL WITH TWO SPATIAL REGIONS

In this section the phenomenon of pseudoreflection of waves from a border between regions of different frequency is briefly investigated in two dimensions. To this end the following two-dimensional FHN model is considered:

$$\frac{\partial \nu}{\partial t} = D\left(\frac{\partial^2 \nu}{\partial x^2} + \frac{\partial^2 \nu}{\partial y^2}\right) + \nu(\nu - a)(1 - \nu) - w,$$

$$\frac{\partial w}{\partial t} = \varepsilon(\nu - dw). \tag{4}$$

Equations (4) were solved on a comparatively large rectangle (150×150 or 150×250 grid points) with Neumann boundary conditions. The medium was divided into two uniform regions, with $\varepsilon = \varepsilon_1$ and $\varepsilon = \varepsilon_2$, $\varepsilon_2 > \varepsilon_1$, respectively, by a straight borderline inclined at an angle θ to the x axis ($0 < \theta < \pi/2$). A plane wave was initiated at the left edge of the low-frequency region (ε_1), moving in the positive x direction. Figure 10 shows that the plane wave is reflected at some angle with respect to the border. The angle of reflection, however, is not equal to the angle of incidence. This inequality is similar to nonlinear reflection (accompanied by second-harmonic generation) of high-powered laser beams [19]. For a larger angle of incidence resulting from a smaller θ, the difference between the angle of incidence and the (smaller) angle of reflection increases [Figs. 10(a) and 11(a)]. Even for an angle of incidence of 90° ($\theta=0$), reflected waves are obtained as shown in Fig. 10(b). The observed difference between the angles of incidence and reflection is not really surprising, since reflection without change of frequency (as in linear optics) is a necessary condition for the equality of angles, while here the frequency of the reflected wave is different than that of the incident wave.

In the ε_1 region, uniform reflected waves of constant wavelength propagate with a fixed angle with respect to the border, whereas in the ε_2 region a wavelength "spreading" is again observed. However, the above-mentioned movement of the "source" of refractive waves now results in the appearance of "target" waves. The source of these waves gradually increases in size, and slowly propagates in the ε_2 region away from the separating line. Following a transient period, the source settles on the "opposite edge" [see, e.g., Fig. 10(a), for $t=48\,000$], similarly to our 1D simulations.

The different wave behavior in the two regions results in "front breaking" in the vicinity of the line of separation, thus satisfying the necessary condition for generation of spirals [20]. Indeed, growing spirals are generated in the higher fre-
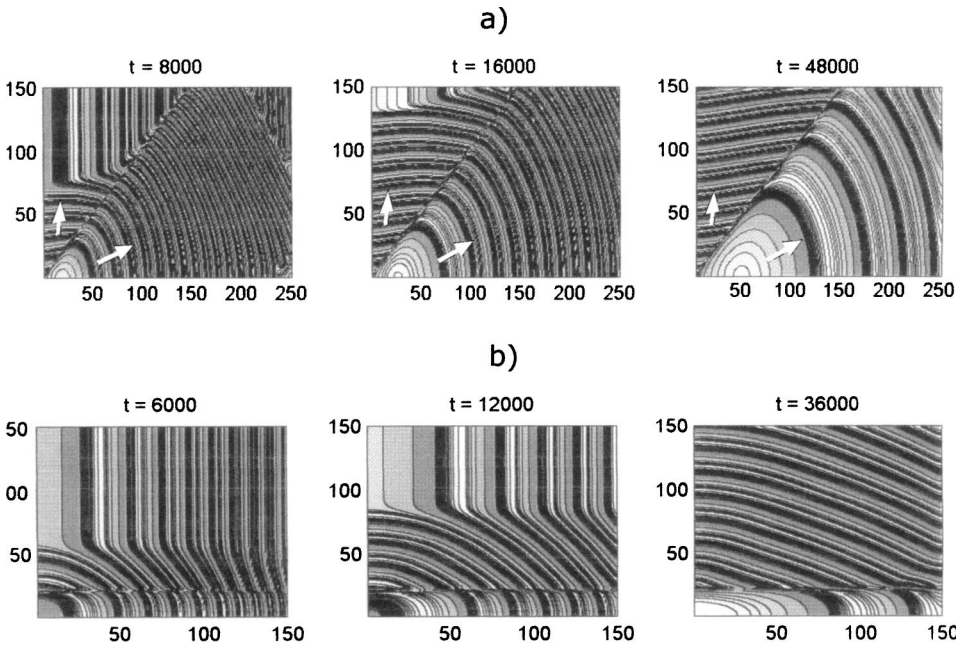

FIG. 10. A two-dimensional gray scale representation of v altitude lines in the range $-0.5 \leqslant v \leqslant 1$ [Eq. (4)]. Abscissa and ordinate values denote indices of grid points. Pseudoreflection of a plane wave, launched in the low-frequency region, is observed on the left boundary. The interface here is a straight line inclined at an angle θ with respect to the x axis. (a) $\theta=63°$; (b) $\theta=0°$. The angle of reflection in both cases is not equal to the angle of incidence. The 2D simulations were performed with $\varepsilon_1=0.03$, $\varepsilon_2=0.05$, and $d=1$, which are different from those used in our 1D simulations. Arrows indicate direction of propagation of the pseudo reflected and refractive waves.
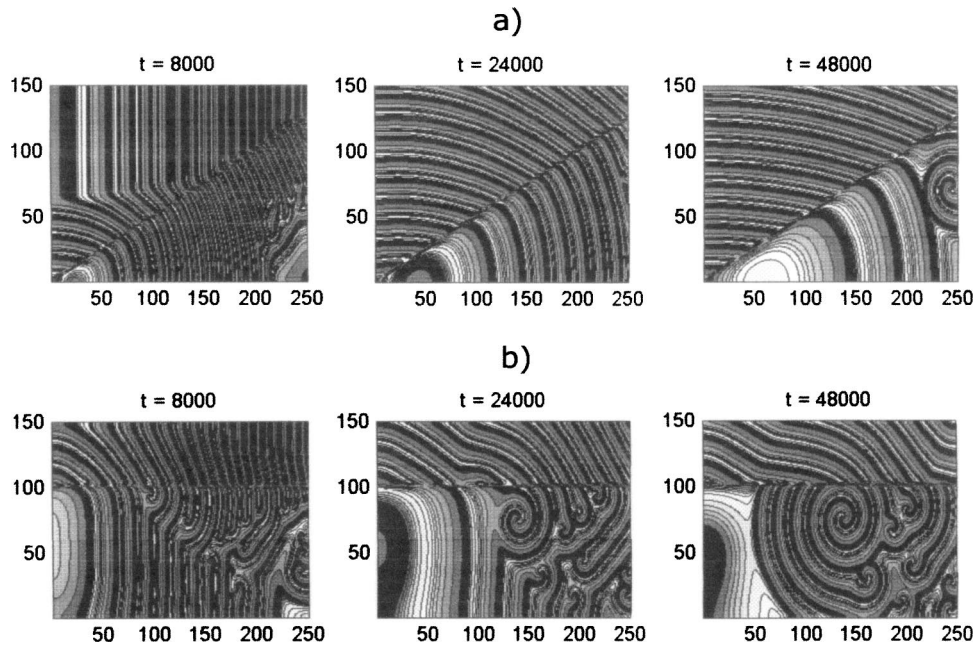
FIG. 11. The dynamics of refractive waves propagated in the 2D high frequency region.　(a) Upper row, $\theta = 37°$; (b) lower row, $\theta = 0°$. Creation of target and spiral waves is observed. The spirals generation strongly depends on the interface orientation θ. The number of spirals drastically increases with a decrease of θ. Gray scale representation of v altitude lines in the range $-0.5 \leq v \leq 1$ [Eq. (4)]. Abscissa and ordinate values denote indices of grid points.

quency (ε_2) region, as shown in Fig. 11. Their appearance is possible only if the angle θ is smaller than some critical value. A further decrease of θ leads to an early appearance of a growing number of spiral waves. Thus $\theta = 0$ is the best situation for spiral generation. Evidently, when the separating line is parallel to the x axis many spirals are observed, Fig. 11(b).

VII. POSSIBLE APPLICATIONS

In this section we wish to emphasize the possibility that the results presented in this work may well be of importance for biological applications. In particular, their relevance to the dynamics of the cardiac sinus node (SN) is discussed. Our simplified model of a SN consists of two embedded LC regions, the inner region being of higher frequency than the outer one, thus preventing the creation of "inward" pseudoreflection [10]. We suggest that this model may contain important features of the dynamical behavior of a sinus node.

It is commonly believed that, despite their nonuniformity, all SN cells oscillate *in unison*, i.e., with the same frequency and zero phase lag [21]. To our knowledge, the existence of propagating waves inside the sinus node has very rarely been discussed previously (see, e.g., [22]). From our simulations, on the other hand, we expect to get out-of-phase motions in the higher-frequency region (Sec. IV) and PRW in its low-frequency region (Sec. II).

The PRW phenomenon itself is interesting in the context of a heart disease called the sinus node reentry [23]. Although as early as 1943 this disturbance was conceived as a potential source of atrial tachycardia [24], the exact description of its dynamics is still problematic. The main problem is that the SN is a rather small organ, thus making electrophysi-

ological measurements very difficult. Nevertheless, sinus echo (ectopic beats inside of the sinus node), which represents an essential part of a reentry circuit was experimentally observed [25] and can probably be explained as some sort of pseudoreflection from an inhomogeneity *within* the SN. A good quantitative comparison, however, would require more precise measurements, as well as more complicated SN models [26].

Figure 9 displays the dependence of the final period of the model SN upon the size of its high frequency region, namely its monotonic decrease with size and an ultimate saturation. Therefore, for a SN composed of two regions with different frequencies, the high frequency region size should be larger than some critical value in order to be able to drive the entire SN at this frequency. This is in addition to our earlier result [9] for a single region SN where the dependence of its final frequency upon its *full* size was shown to be strongly nonmonotonic. The exact SN structure remains an open problem to this day. Along with the model examined in this work, including a simple piecewise *constant* nonuniformity, the so-called "gradient model" in which more complex, piecewise *linear* nonuniformities is also quite popular [27]. We have therefore performed some FHN numerical simulations with piecewise linear nonuniformities and found a similar effect of pseudoreflection as described above.

Another interesting result is the diffusion-induced bifurcations in the transient zones near the interface. Besides the obvious theoretical interest which this phenomenon arouses, it could allow a better understanding of the influence of the coupling between SN cells upon the development of cardiac arrhythmias. In particular, it was shown that some of cardiac arrhythmias may arise as a result of a poor intercellular coupling in the sinus node [28]. Here we demonstrated the op-

posite effect, namely, that enhanced coupling can also lead to cardiac arrhythmias. Indeed, our simulations (Sec. III) imply that an increase in the diffusion coefficient D (i.e., in the coupling between oscillating points) leads to a size increase of the transient zone of the low-frequency region which can extend even as far as the SN boundary. Thus complex periodic oscillations [similar to those presented in Figs. 6(a) and 6(b)] could appear at the SN output, a phenomenon which can destroy normal cardiac functioning.

Spiral-waves generation in our 2D simulations is usually associated with serious arrhythmias in the heart [29,30]. Section VI of this work presents a specific mechanism for such spiral generation, namely the superposition of 2D uniform SN regions at certain orientation to each other. The geometry of the different parts of the SN therefore plays a critical role. Our results show, e.g., that the optimal orientation of the interface in order to avoid spiral waves is for it to be perpendicular to the propagating waves direction.

[1] L. Glass and M. C. Mackey, *From Clocks to Chaos: The Rhythms of Life* (Princeton University Press, Princeton, NJ, 1988).

[2] J. Honerkamp, J. Math. Biol. **18**, 69 (1983).

[3] E. Marder and R. L. Calabrese, Physiol. Rev. **76**, 687 (1996).

[4] A. Ylinen *et al.*, J. Neurosci. **15**, 30 (1995).

[5] R. R. Aliev, W. Richards, and J. P. Wikswo, J. Theor. Biol. **204**, 21 (2000).

[6] A. Sherman, in *Case Studies in Mathematical Modeling: Ecology, Physiology, and Cell Biology*, edited by H. G. Othmer, F. R. Adler, M. A. Lewis, and J. C. Dallon (Prentice-Hall, New York, 1997), p. 199.

[7] G. A. Oda *et al.*, J. Theor. Biol. **206**, 515 (2000).

[8] E. Ben-Jacob *et al.*, Nature (London) **373**, 566 (1995).

[9] A. Rabinovitch, M. Gutman, and I. Aviram, Phys. Rev. E **67**, 036212 (2003).

[10] A. Rabinovitch, M. Gutman, and I. Aviram, J. Biol. Phys. **28**, 713 (2002).

[11] R. FitzHugh, Biophys. J. **1**, 445 (1961).

[12] A. Rabinovitch *et al.*, J. Theor. Biol. **196**, 141 (1999).

[13] S. H. Strogatz, *Nonlinear Dynamics and Chaos: With Applications to Physics, Biology, Chemistry and Engineering* (Addison-Wesley, Reading, MA, 1994).

[14] Y. Kuramoto, *Chemical Oscillations, Waves and Turbulence* (Springer, Berlin, 1984).

[15] P. Ortoleva and J. Ross, J. Chem. Phys. **58**, 5673 (1973).

[16] B. Barnes and R. Grimshaw, Int. J. Bifurcation Chaos Appl. Sci. Eng. **7**, 2653 (1997).

[17] S. Doi and S. Sato, Math. Biosci. **125**, 229 (1995).

[18] J. Keener and L. Glass, J. Math. Biol. **21**, 175 (1984).

[19] J. Ducuing and N. Bloembergen, Phys. Rev. Lett. **10**, 474 (1963).

[20] A. T. Winfree, *The Geometry of Biological Time* (Springer-Verlag, Berlin, 1990).

[21] J. Jalife, J. Physiol. (London) **356**, 221 (1984).

[22] H. Zhang, A. V. Holden, and M. R. Boyett, Nonlinear Anal. Theory, Methods Appl. **30**, 1019 (1997).

[23] J. E. Olgin, in *Cardiac Electrophysiology: From Cell to Bedside*, 3rd ed., edited by D. P. Zipes and J. Jalife (Saunders, Philadelphia, 2000), p. 459.

[24] P. Barker, F. Wilson, and D. Johnston, Am. Heart J. **26**, 435 (1943).

[25] M. A. Allesie and F. I. Bonke, Circ. Res. **44**, 557 (1979).

[26] H. Irisawa and A. Noma, in *Cardiac Rate and Rhythm*, edited by L. N. Bouman and H. J. Jongsma (Nijhoff, The Hague, 1982), p. 35.

[27] H. Zhang, A. V. Holden, and M. R. Boyett, Circulation **103**, 584 (2001).

[28] P. Östborn, B. Wohlfart, and G. Ohlén, J. Theor. Biol. **211**, 201 (2001).

[29] V. Krinsky, Pharm. Ther. B **3**, 593 (1978).

[30] A. V. Holden, Nature (London) **387**, 655 (1997).